Science Robotics
AAAS

Supplementary Materials for

Submillimeter-scale multimaterial terrestrial robots

Mengdi Han *et al.*

Corresponding author: Yonggang Huang, y-huang@northwestern.edu; Yihui Zhang, yihuizhang@tsinghua.edu.cn; John A. Rogers, jrogers@northwestern.edu

Sci. Robot. **7**, eabn0602 (2022)
DOI: 10.1126/scirobotics.abn0602

The PDF file includes:

Supplementary Methods
Figs. S1 to S38
Table S1
Legends for movies S1 to S12
References (*43*–*62*)

Other Supplementary Material for this manuscript includes the following:

Movies S1 to S12

1. Supplementary Methods

Method S1: Step-by-step fabrication procedures for 3D robots constructed in SMA and a single layer of PI

Preparation of the substrate

1. Prepare Si wafers with Cr (sputtered, thickness: 50 nm) and SMA (sputtered, thickness: 2.5 μm)
2. Anneal sample at 500 °C in vacuum for 30 min
3. Clean sample with acetone and IPA

Pattern the SMA

4. Define SMA pattern using photoresist (S1813, speed: 4000 rpm, time: 60 s, ramp: 500 rpm/s)
5. Etch SMA with HNO_3:HF:H_2O (1:1:10)
6. Remove photoresist with acetone

Pattern the PI

7. Spin coat PI2545 (800 rpm, 40 s; bake at 110 °C for 180 s, 150 °C for 300 s; fully cure)
8. Deposit Cu (thickness: 100 nm)
9. Define Cu pattern using photoresist (S1813, speed: 4000 rpm, time: 60 s, ramp: 500 rpm/s)
10. Etch Cu with copper etchant (Transene Company, Inc.; Copper Etchant CE-100; Ferric Chloride 25-35 wt%, Hydrochloric Acid 3-4 wt%, Water >60 wt%)
11. Oxygen plasma etching of PI2545 (Cu and SMA pattern serve as the etching mask)
12. Etch Cr with chromium etchant (Transene Company, Inc.; Chromium Etchant CEP-200; Perchloric Acid 6 wt%, Cerric Ammonium Nitrate 9 wt%, Water 75 wt%. Cu also dissolves in chromium etchant)

Transfer printing, buckling, and releasing

13. Transfer 2D precursors of robots to water soluble tape
14. Deposit SiO_2 (thickness: 100 nm) with a shadow mask to define the bonding sites for buckling
15. Ultraviolet ozone (UVO) treatment (intensity: 28-32 mW/cm², wavelength: 253.7 nm) of silicone (Dragon Skin) and 2D precursors of robots for 4 min;
16. Transfer 2D precursors of robots onto pre-stretch silicone
17. Heat in the oven at 70 ˚C for 8 min, remove water soluble tape with water
18. Release prestrain to form 3D robots
19. Conformally deposit SiO_2 (thickness: 1 μm) on 3D robots and the silicone substrate
20. Dissolve the silicone substrate in Dynasolve
21. Apply sonication to remove freestanding SiO_2

Method S2: Step-by-step fabrication procedures for 3D robots constructed in SMA and a double layer of PI

Preparation of the substrate

1. Prepare Si wafers with Cr (sputtered, thickness: 50 nm) and SMA (sputtered, thickness: 2.5 μm)
2. Anneal sample at 500 °C in vacuum for 30 min
3. Clean sample with acetone and IPA

Pattern the SMA

4. Define SMA pattern using photoresist (S1813, speed: 4000 rpm, time: 60 s, ramp: 500 rpm/s)
5. Etch SMA with HNO_3:HF:H_2O (1:1:10)
6. Remove photoresist with acetone

Pattern the 1st PI layer

7. Spin coat PI2545 (800 rpm, 40 s; bake at 110 °C for 180 s, 150 °C for 300 s; fully cure)
8. Deposit Cr/Au (thickness: 10 nm/100 nm)
9. Define Au pattern using photoresist (S1813, speed: 4000 rpm, time: 60 s, ramp: 500 rpm/s)
10. Etch Au with gold etchant (Transene Company, Inc.; Gold Etchant Type TFA; Iodine Complex 8 wt%, Potassium Iodide 21 wt%, Water 71 wt%.)
11. Peel off PI from the Si wafer (all materials, except the Si wafer, will attach to the PI layer)
12. Etch Cr with chromium etchant (Transene Company, Inc.; Chromium Etchant CEP-200; Perchloric Acid 6 wt%, Cerric Ammonium Nitrate 9 wt%, Water 75 wt%.)
13. Remove photoresist with acetone

Pattern the 2nd PI layer

14. Spin coat PDMS (3000 rpm, 1:10) on glass slide
15. Attach sample to PDMS (PI layer facing down)
16. Spin coat PI2545 (3000 rpm, 40 s; bake at 110 °C for 180 s, 150 °C for 300 s; fully cure)

Pattern the PI

17. Peel off PI from PDMS
18. Attach sample to another PDMS coated glass (1st thick PI layer facing up)
19. Oxygen plasma etching of PI2545 (Au/Cr and SMA pattern serve as the etching mask)
20. Etch Au and Cr with gold and chromium etchant

Transfer printing, buckling and releasing

21. Transfer 2D precursors of robots to water soluble tape (1st thick PI layer facing up)
22. Deposit SiO_2 (100 nm in thickness) with a shadow mask to define the bonding sites for buckling

23. UVO (intensity: 28-32 mW/cm², wavelength: 253.7 nm) treatment of silicone (Dragon Skin) and 2D precursors of robots for 4 min;
24. Transfer 2D precursors of robots onto pre-stretch silicone
25. Heat in the oven at 70 ˚C for 8 min, remove water soluble tape with water
26. Release prestrain to form 3D robots
27. Conformally deposit SiO_2 (thickness: 1 μm) on 3D robots and the silicone substrate
28. Dissolve the silicone substrate (Dynasolve 230, DYNALOY)
29. Apply sonication to remove freestanding SiO_2

Method S3: Step-by-step fabrication procedures for the 3D robots constructed in SMA

Preparation of the substrate

1. Prepare Si wafers with Cr (sputtered, thickness: 50 nm) and SMA (sputtered, thickness: 2.5 μm)
2. Anneal sample at 500 °C in vacuum for 30 min
3. Clean sample with acetone and IPA

Pattern the SMA

4. Define SMA pattern using photoresist (S1813, speed: 4000 rpm, time: 60 s, ramp: 500 rpm/s)
5. Etch SMA with HNO_3:HF:H_2O (1:1:10)
6. Remove photoresist with acetone

Transfer printing, buckling, and releasing

7. Transfer 2D precursors of robots to water soluble tape
8. Deposit SiO_2 (thickness: 100 nm) with a shadow mask to define the bonding sites for buckling
9. UVO treatment (intensity: 28-32 mW/cm², wavelength: 253.7 nm) of silicone (Dragon Skin) and 2D precursors of robots for 4 min;
10. Transfer 2D precursors of robots onto pre-stretch silicone
11. Heat in the oven at 70 ˚C for 8 min, remove water soluble tape with water
12. Release prestrain to form 3D robots
13. Conformally deposit SiO_2 (thickness: 1 μm) on 3D robots and the silicone substrate
14. Dissolve the silicone substrate in Dynasolve
15. Apply sonication to remove freestanding SiO_2

Method S4: Constitutive model of the shape memory alloy

The relationship between strain, stress, temperature and crystallographic phase of shape memory alloy (SMA) material in this manuscript was described by the Brinson thermo-constitutive model, as given by Ref. (*43*):

$$d\sigma = D(\varepsilon, \xi, T)d\varepsilon + \Omega(\varepsilon, \xi, T)d\xi + \Theta(\varepsilon, \xi, T)dT.$$

Here, D, Ω and Θ are the stiffness, phase transformation coefficient and thermal expansion coefficient of shape memory alloy. The stress can be also referred to the strain ε, martensite fractions ξ and temperature T as

$$\sigma - \sigma_0 = D(\xi)\varepsilon - D(\xi_0)\varepsilon_0 + \Omega(\xi)\xi - \Omega(\xi_0)\xi_0 + \Theta(T - T_0),$$

where σ_0, ε_0, ξ_0 and T_0 represent the values at the initial state, while σ, ε, ξ and T are the real-time state of SMA material. It is important to note that the application of a specific material restriction enforces a relationship between the stiffness and phase transformation coefficient. Considering the initial condition of $\sigma_0 = \varepsilon_0 = \xi_0 = 0$ and final condition of $\sigma_0 = 0$, $\varepsilon = \varepsilon_L$, $\xi = 1$, the phase transformation coefficient Ω can be given as:

$$\Omega = -D\varepsilon_L,$$

where ε_L is the maximum recoverable strain, and can be determined by the onset value that all of the original austenite are completely detwinned martensite.

For the final state ($\sigma_0 = 0$, $\xi_0 = 1$, $\varepsilon_0 = \varepsilon_L$), the strain and stress relationship in SMA is:

$$\varepsilon = \frac{?}{\xi E_m + (1-\xi)E_a} + \varepsilon_L \xi,$$

where E_m and E_a refer to the Young's modulus of SMA in the austenite and the martensite phase, respectively. The martensite fraction ξ during the phase transformation from martensite to austenite (heating) can be described as follows:

$$\xi = \frac{\xi_M}{2}\left(\cos\left[\frac{\pi(T - A_S)}{A_f - A_S} - \frac{\pi\sigma}{C_A(A_f - A_S)}\right] + 1\right).$$

And during the phase transformation from austenite to martensite (cooling), the martensite fraction ξ is

$$\xi = \frac{1-\xi_A}{2}\left(\cos\left[\frac{\pi(T - M_f)}{M_s - M_f} - \frac{\pi\sigma}{C_M(M_s - M_f)}\right] + \frac{1+\xi_A}{2}\right),$$

where ξ_M is the minimum martensite fraction equal to ξ_0, assumed to be 1 in this case; and C_A and C_M are the dimensionless curve-fitting parameters. A_s and A_f represent the starting and finishing temperatures of the phase transformation from martensite to austenite, while M_s and M_f are the ones of the phase transformation from austenite to martensite.

2. Supplementary Figures

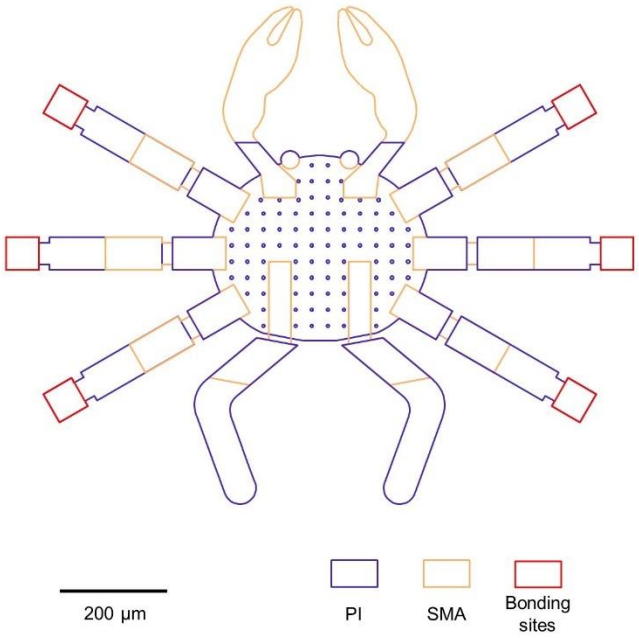

Fig. S1. 2D layout of the crab structure.

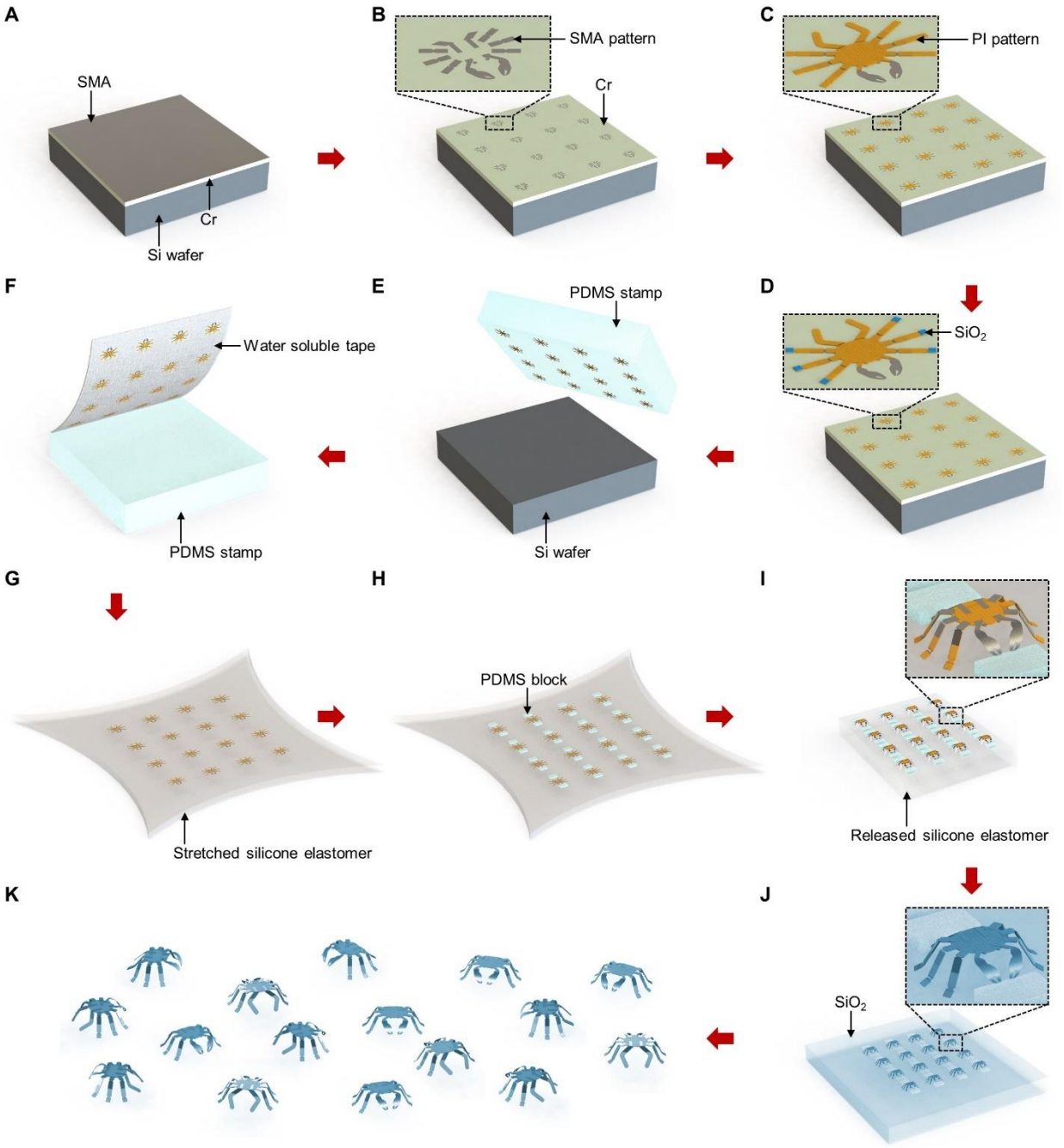

Fig. S2. Schematic illustration of the fabrication procedures for the 3D crab. (**A**) Si wafer with Cr and SMA. (**B**) Pattern the SMA. (**C**) Spin coat and define the PI pattern. (**D**) Deposit and pattern SiO_2. (**E**) Undercut Cr and transfer the 2D precursors to a PDMS stamp. (**F**) Transfer the 2D precursors to a water soluble tape. (**G**) Transfer the 2D precursors to a prestretched elastomer. (**H**) Transfer the PDMS block. (**I**) Compressive buckling. (**J**) Conformally deposit the SiO_2. (**K**) Dissolve the silicone.

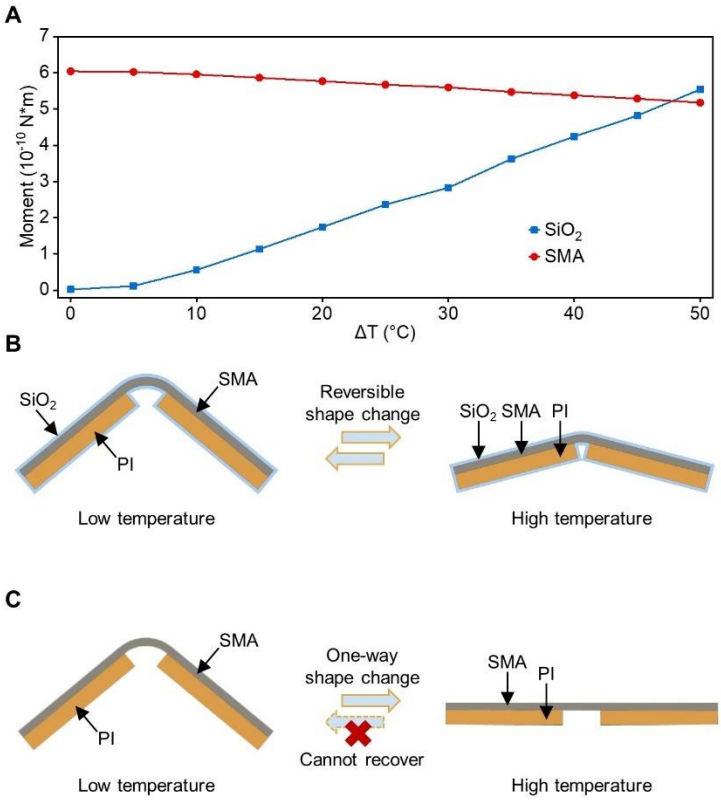

Fig. S3. Functions of the SiO_2 shell. (**A**) Simulation results of the driving force of SMA and elastic force of SiO_2 shell during actuation. (**B**) Reversible shape change of the 3D robot with the SiO_2 shell. (**C**) One-way shape change of the 3D robot without the SiO_2 shell.

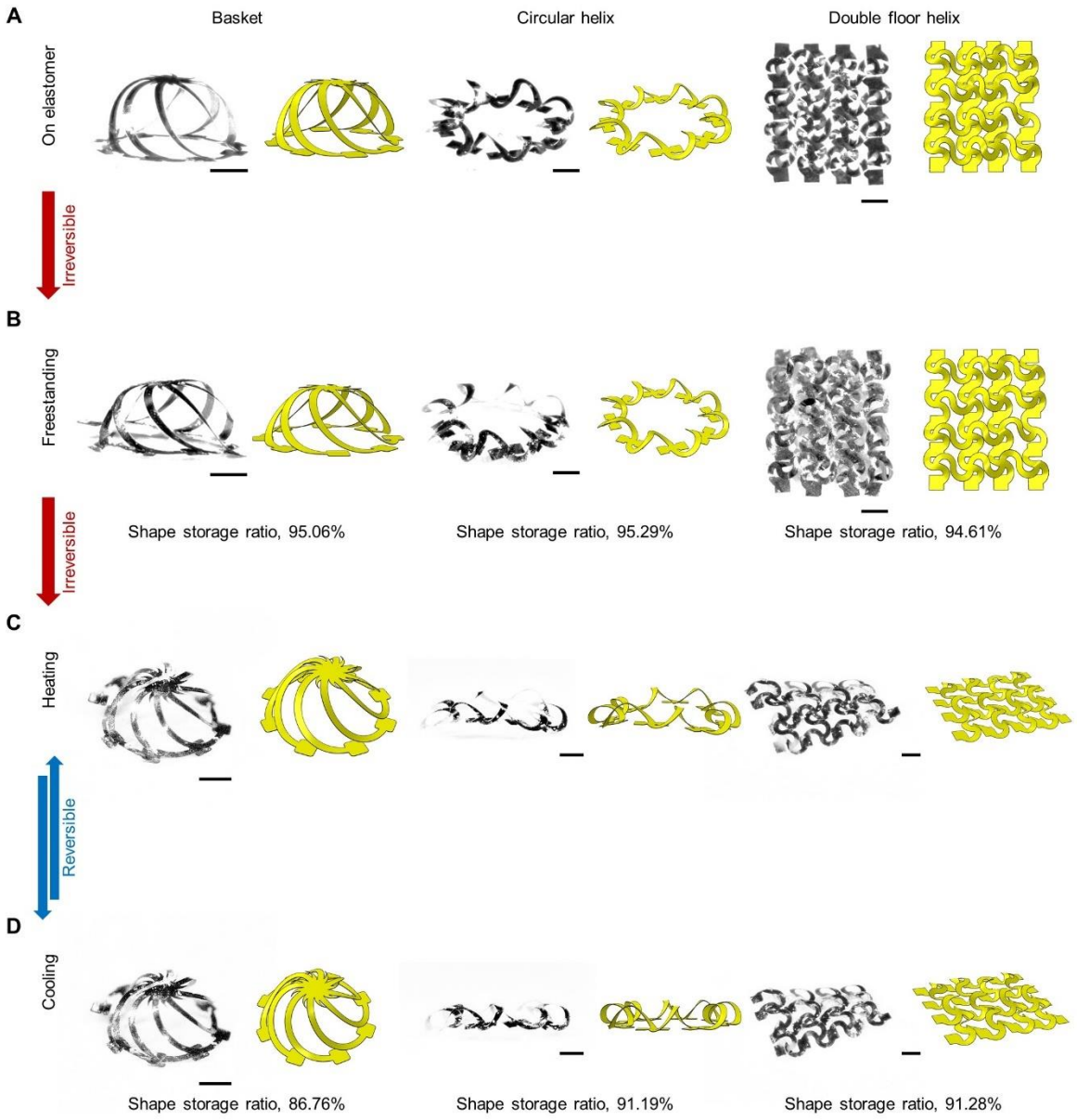

Fig. S4. Experimental and FEA results of various 3D robots at different stages. (**A**) Geometries of 3D robots on an elastomer substrate. (**B**) Geometries of freestanding 3D robots after release from the elastomer. (**C**) Geometries of freestanding 3D robots under global heating. (**D**) Geometries of freestanding 3D robots after cooling to room temperature. Scale bars, 200 μm.

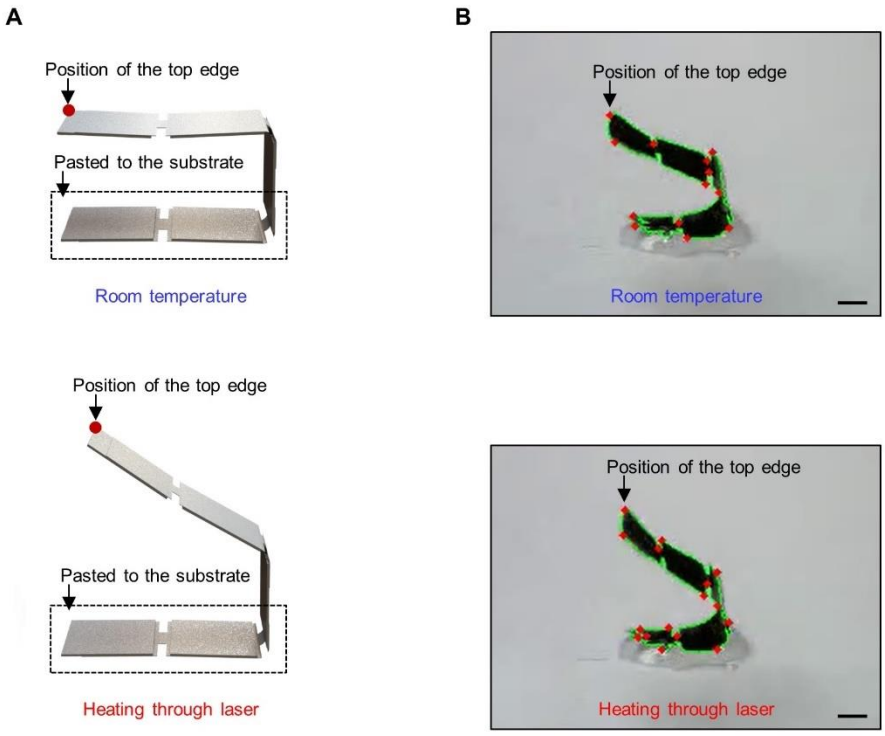

Fig. S5. Stability of reversible actuation. (**A**) Schematic illustration of the setup. (**B**) Optical image of the 3D ribbon pasted to the substrate, with detected edges (green lines) and nodes (red dots). Scale bars, 200 μm.

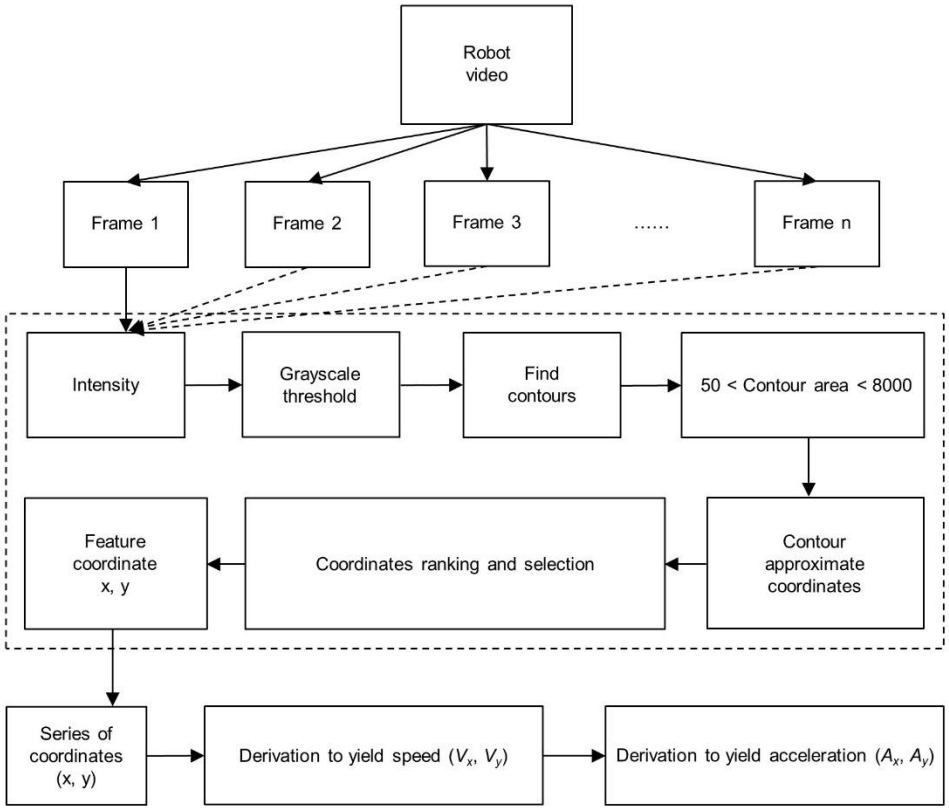

Fig. S6. Algorithm to calculate the position, speed, and acceleration of robots from video recordings.

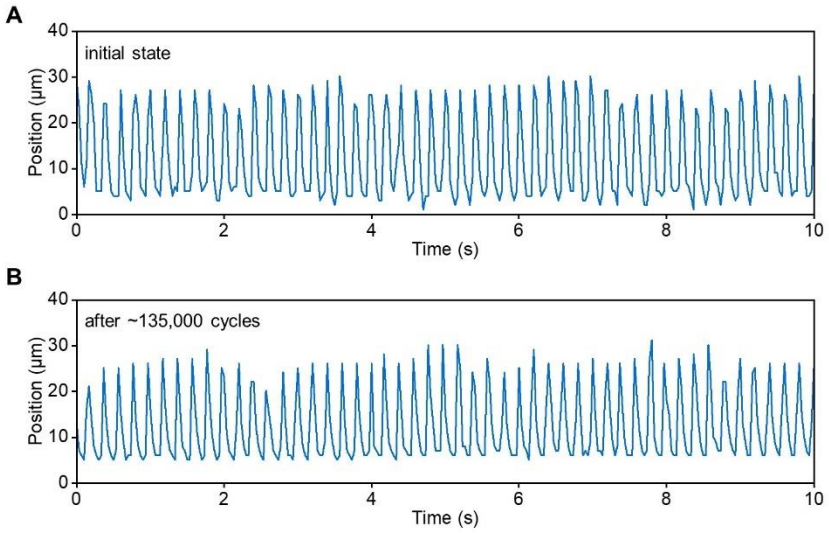

Fig. S7. Stability of the 3D ribbon under cyclic heating and cooling. (**A**) Position of the top edge of the 3D ribbon at the initial state. (**B**) Position of the top edge of the 3D ribbon after ~135,000 cycles.

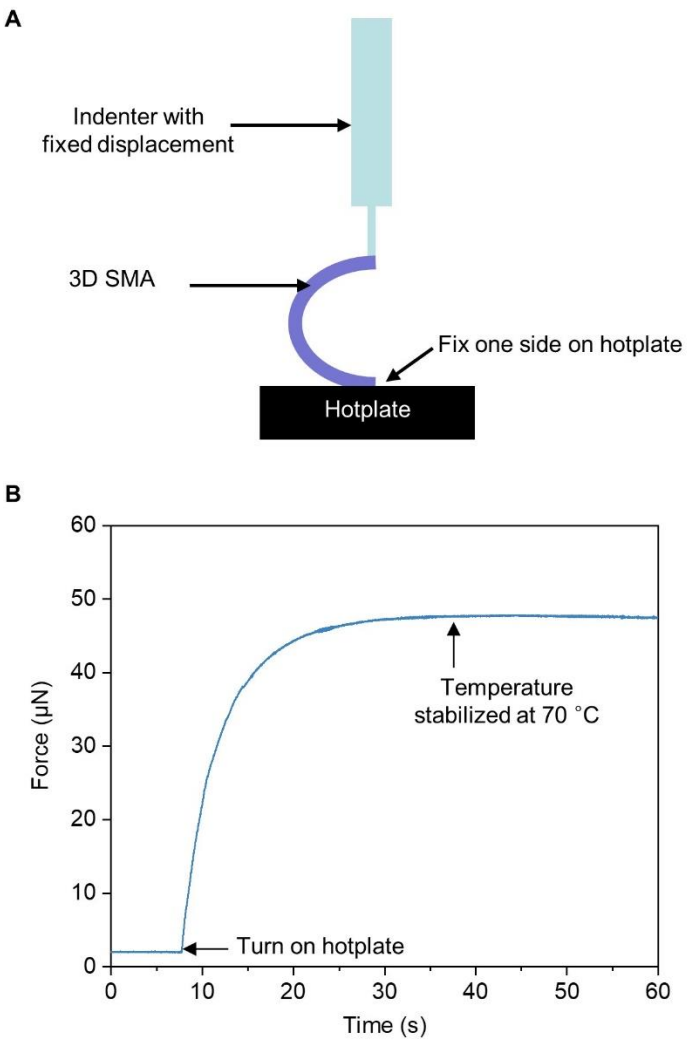

Fig. S8. Measurement of the force generated from a 3D SMA ribbon. (**A**) Schematic illustration of the testing setup. (**B**) Force as a function of time during heating.

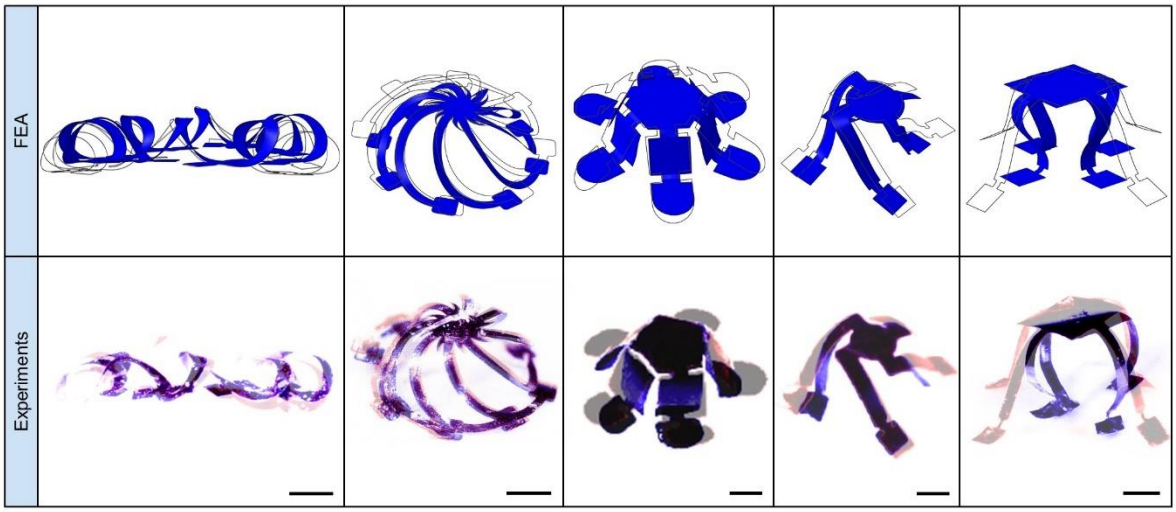

Fig. S9. Superimposed images of various 3D robotic structures. Top: FEA results; images with blue color and black lines correspond to 3D geometries at room temperature and ~100 °C, respectively. Bottom: experimental results; images colorized with blue and red colors correspond to 3D geometries at room temperature and elevated temperature (~100 °C), respectively. Scale bars, 200 μm.

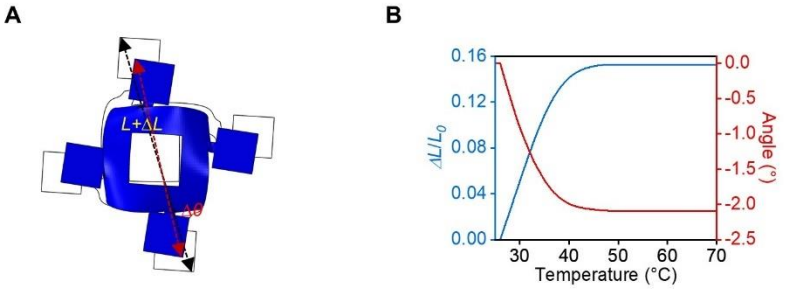

Fig. S10. FEA results of the displacements and twisting angles of a representative 3D robot. (**A**) Schematic illustration. (**B**) Displacements and twisting angles at different temperatures.

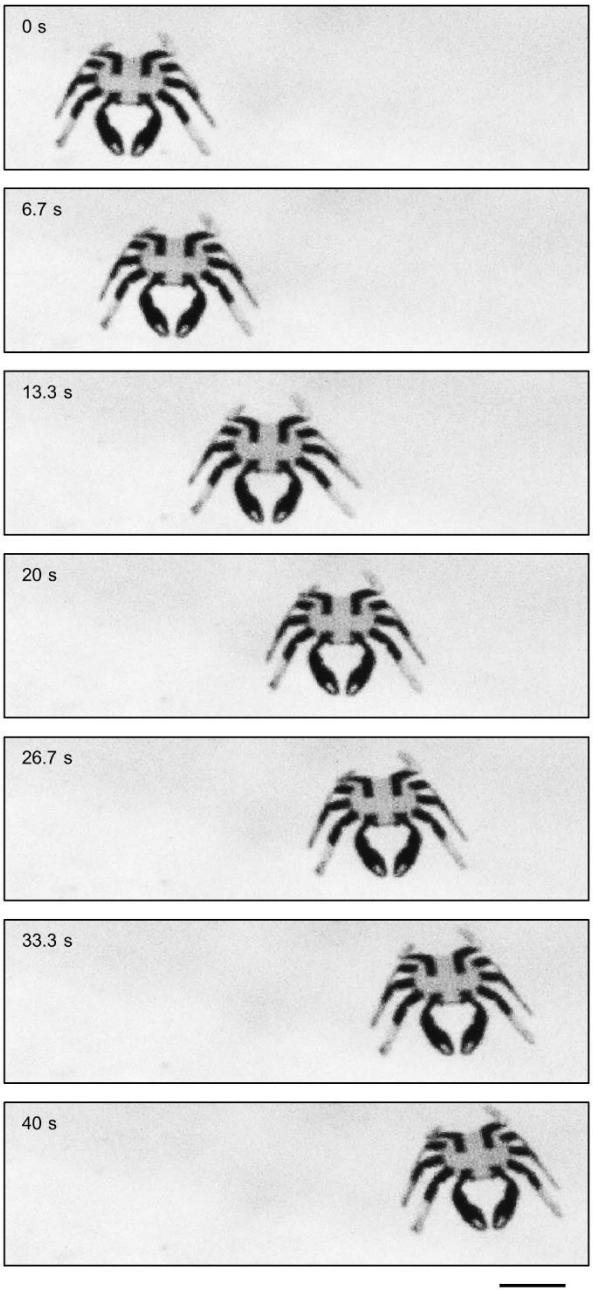

Fig. S11. Optical images of a 3D crab structure during laser-scanning at a frequency of 4 Hz. Scale bar, 500 μm.

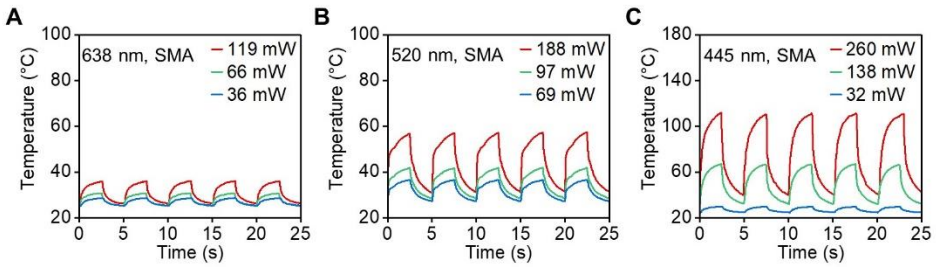

Fig. S12. Time-domain temperature responses of the planar SMA structure to laser irradiation at different wavelengths. (**A**) 638 nm, (**B**) 520 nm, and (**C**) 445 nm wavelengths. The laser scanning frequency and duty cycle are 0.2 Hz and 50% (square wave), respectively.

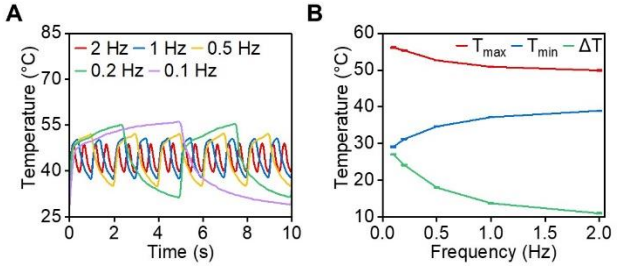

Fig. S13. Temperatures of a planar, suspended SMA ribbon under laser irradiation at different frequencies. (**A**) Time-domain temperature response. (**B**) Maximum temperature, minimum temperature, and temperature difference as a function of frequencies. Wavelength: 520 nm; power: 188 mW; duty cycle: 50% square wave.

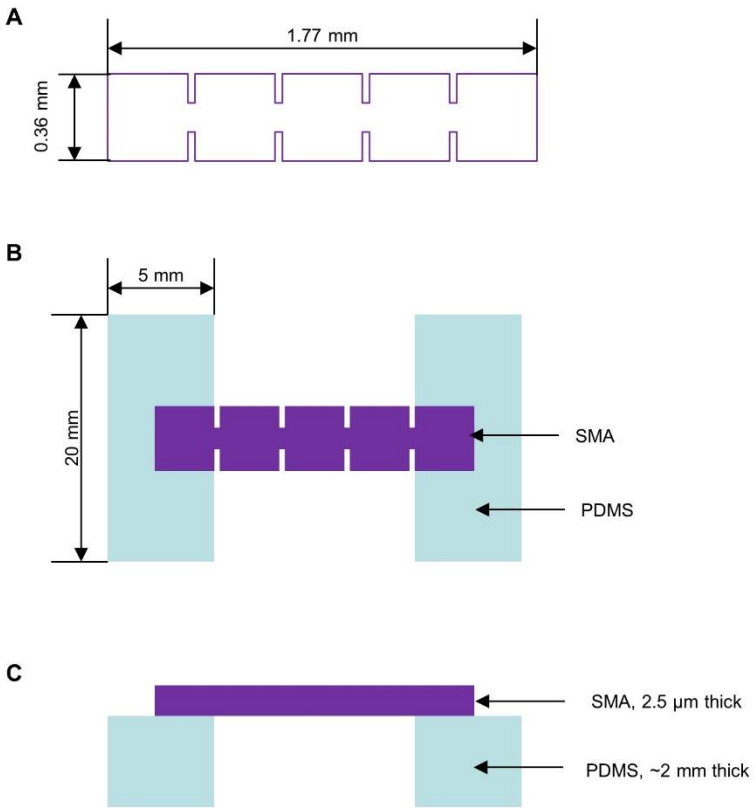

Fig. S14. Schematic illustration of the 2D precursor used for the measurement of temperature. (**A**) Shape and dimensions of the 2D precursor. (**B-C**) Top view (B) and side view (C) of the 2D precursor attached to PDMS supporting structures.

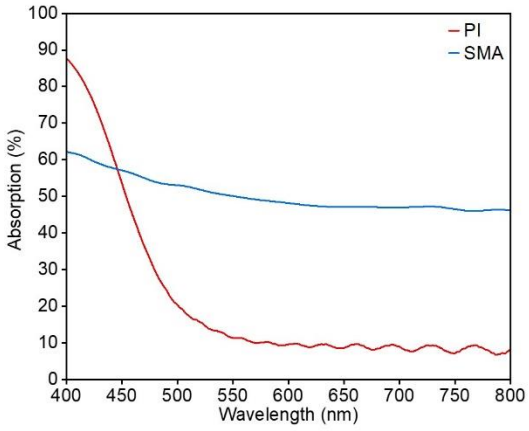

Fig. S15. Absorption spectrum of SMA (~2.5 μm in thickness) and PI (~8 μm in thickness).

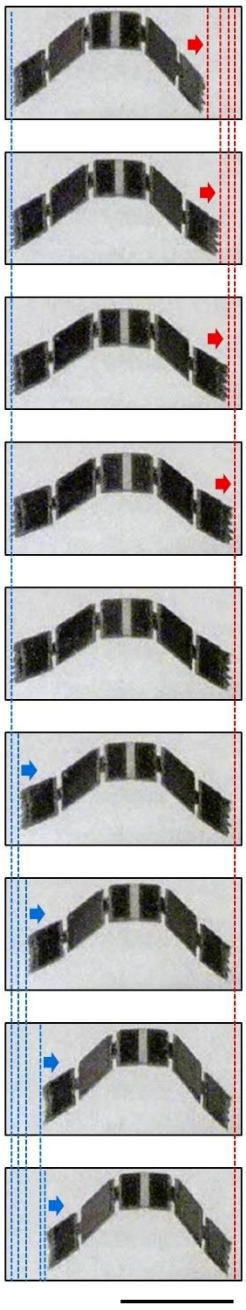

Fig. S16. Optical images showing the asynchronous movement of the left and right ends of a 3D ribbon during laser-scanning at a frequency of 0.1 Hz. Scale bar, 500 μm. Frame interval: 0.3 s.

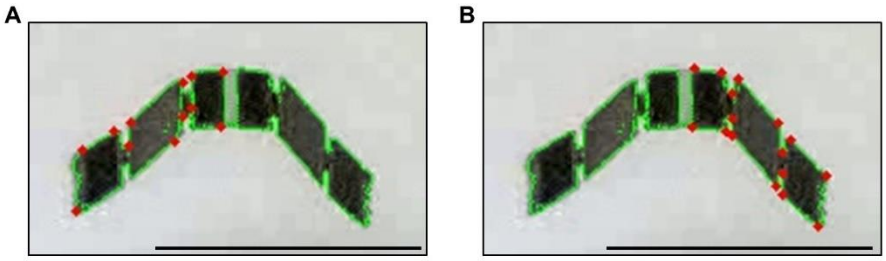

Fig. S17. Edges (green lines) and nodes (red dots) of the 3D ribbon detected from the algorithm. (**A**) Left part. (**B**) Right part. Scale bars, 1 mm.

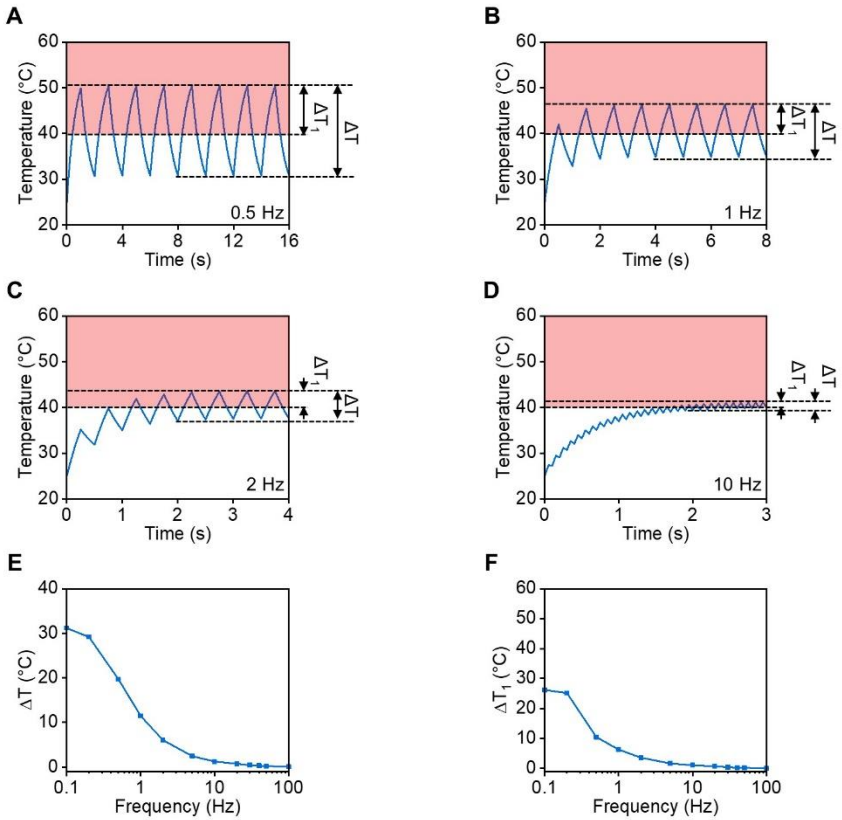

Fig. S18. FEA results of the temperature on the 3D ribbon structure. (**A-D**)**,** Time-domain temperature curves at laser scanning frequencies of 0.5 (A), 1 (B), 2 (C), and 10 Hz (D). The temperature that triggers the phase transition of the SMA and the temperature above which the phase transition ceases are set to 40 °C and 75 °C, respectively. Therefore, only temperature changes between 40 to 75 °C (indicated with red background in (A-D)) are effective (defined as ΔT_1). (**E**) ΔT at different laser scanning frequencies. (**F**) ΔT_1 (i.e. effective ΔT) at different laser scanning frequencies.

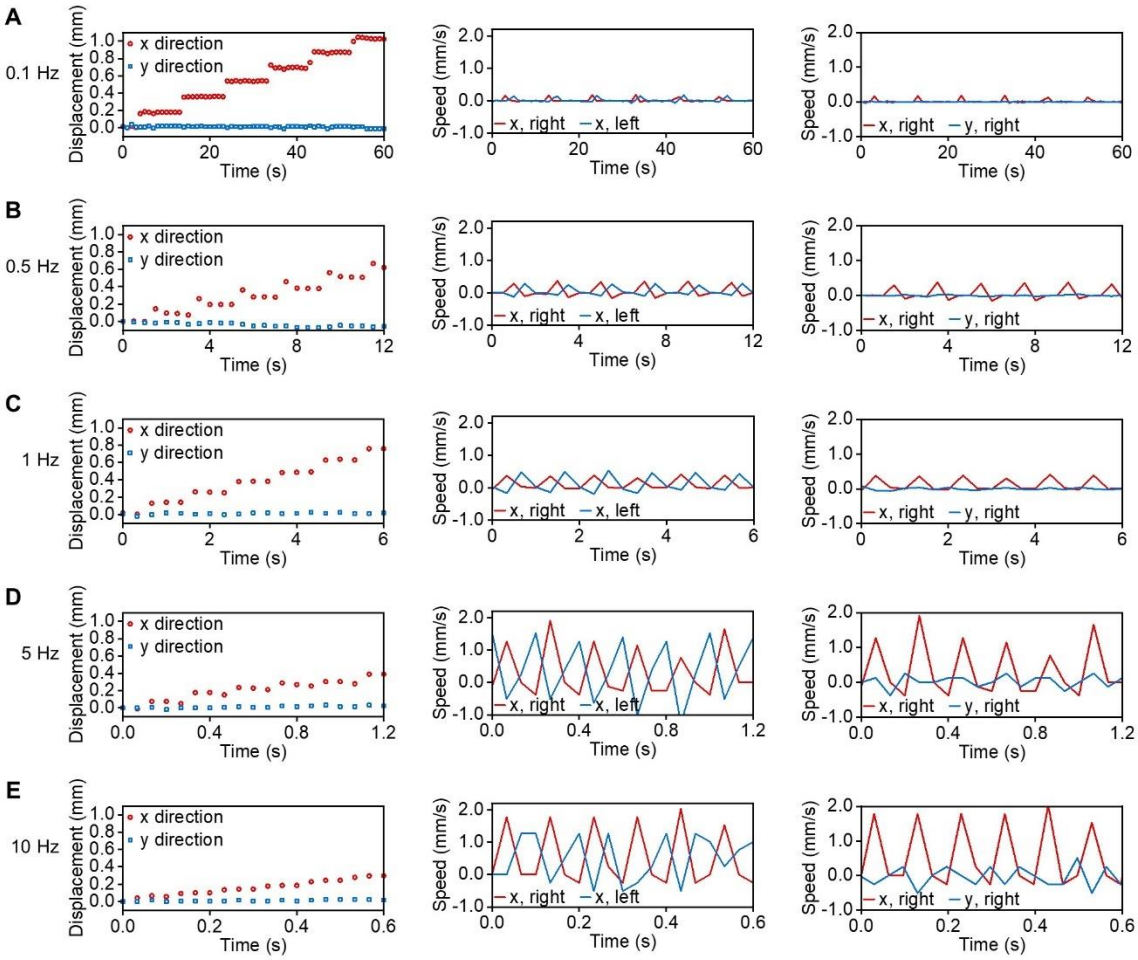

Fig. S19. Additional results of displacements and speeds of a ribbon robot under different laser-scanning frequencies. (**A**) 0.1 Hz. (**B**) 0.5 Hz. (**C**) 1 Hz. (**D**) 5 Hz. (**E**) 10 Hz.

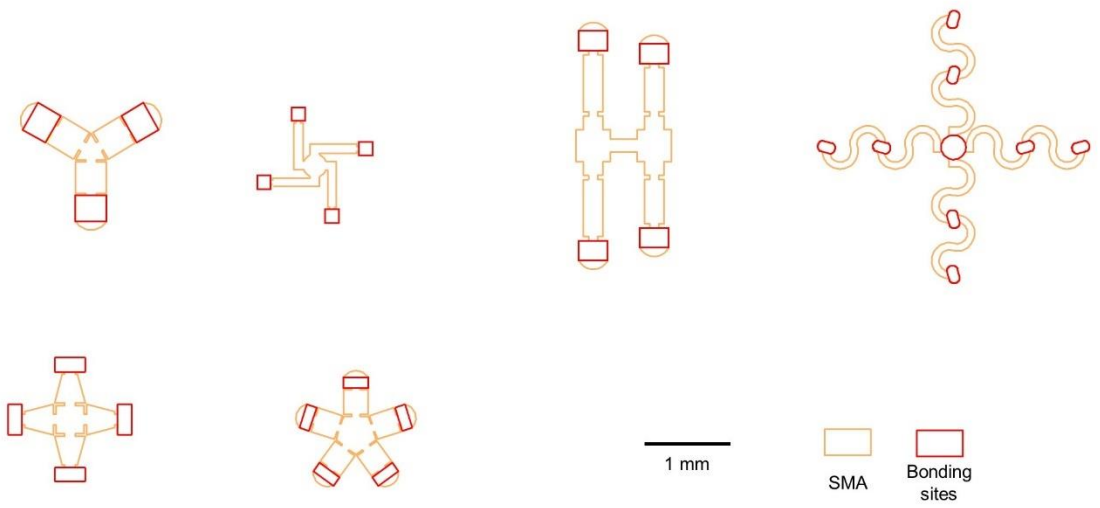

Fig. S20. 2D layouts of robots constructed in SMA.

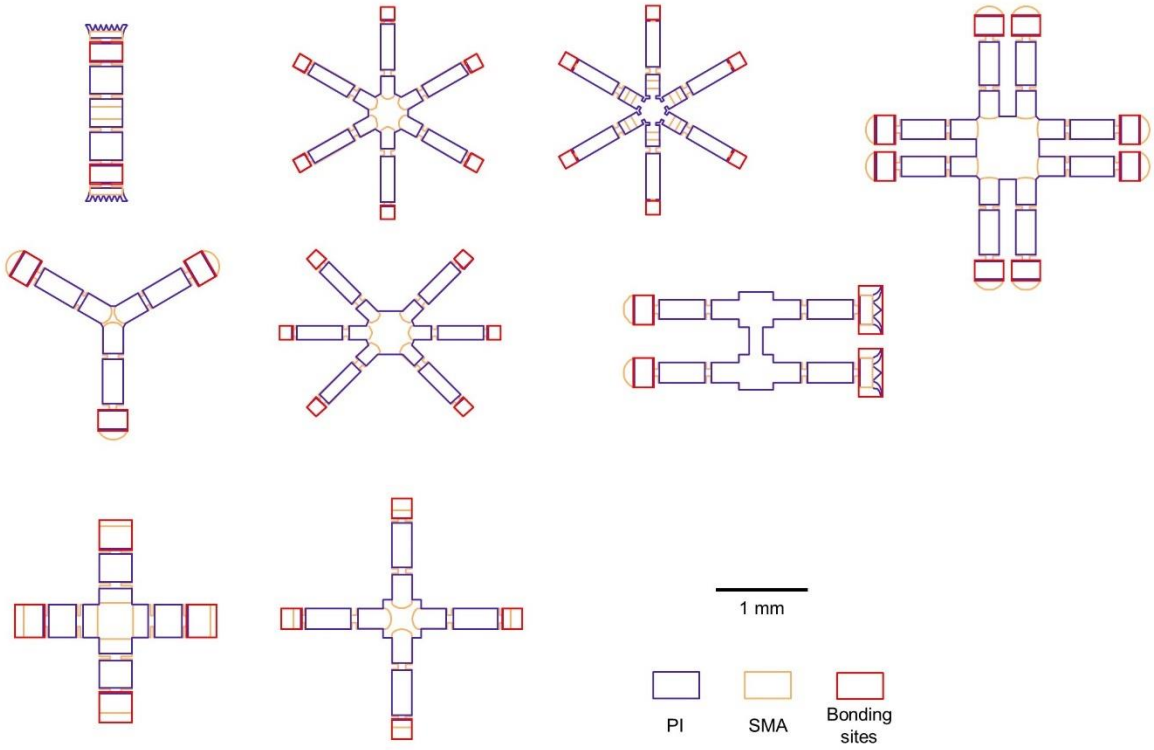

Fig. S21. 2D layouts of robots constructed in PI and SMA.

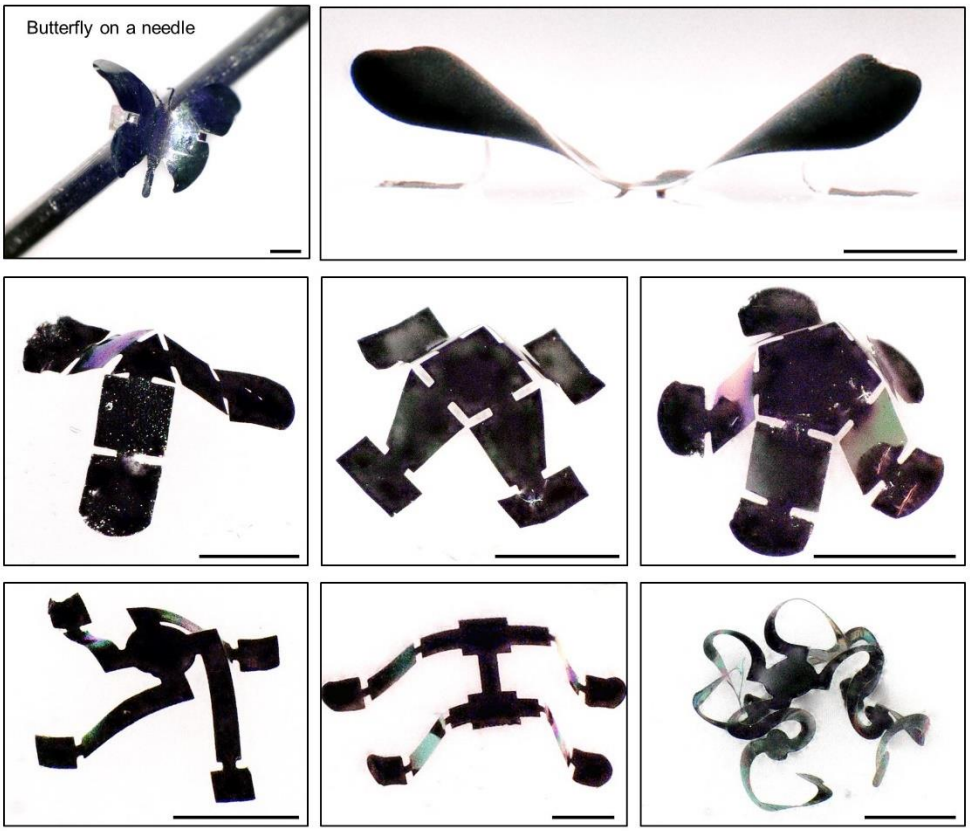

Fig. S22. Optical images of various robots constructed in SMA. Scale bars, 500 μm.

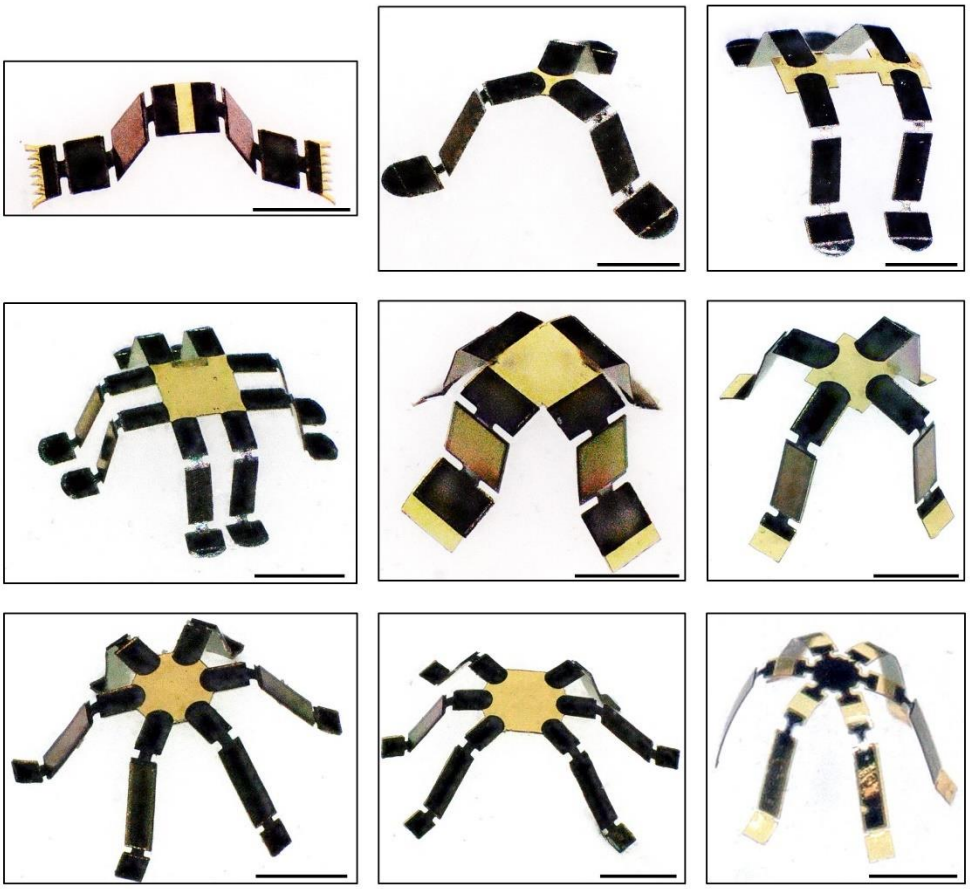

Fig. S23. Optical images of various robots constructed in SMA and PI. Scale bars, 500 μm.

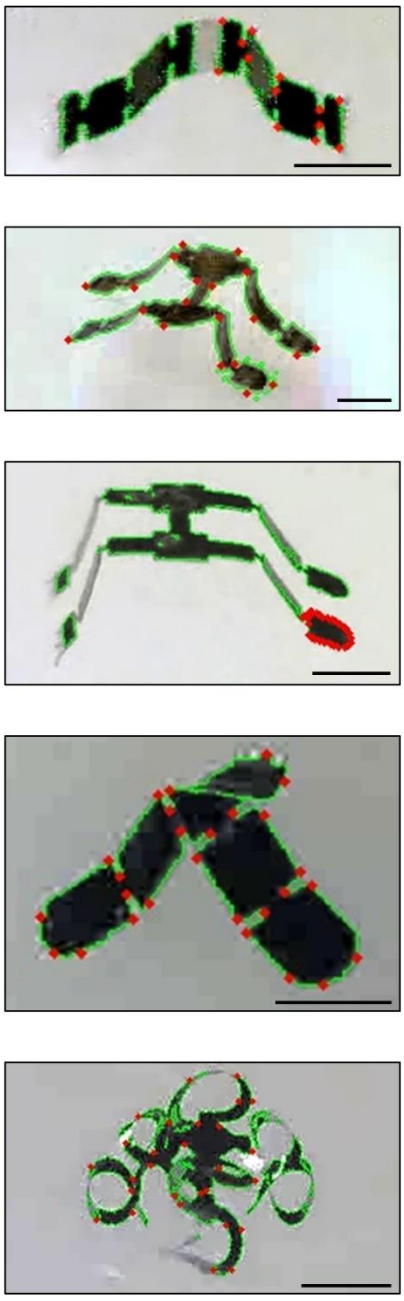

Fig. S24. Edges (green lines) and nodes (red dots) of different 3D robots detected from the algorithm. Scale bars, 500 μm.

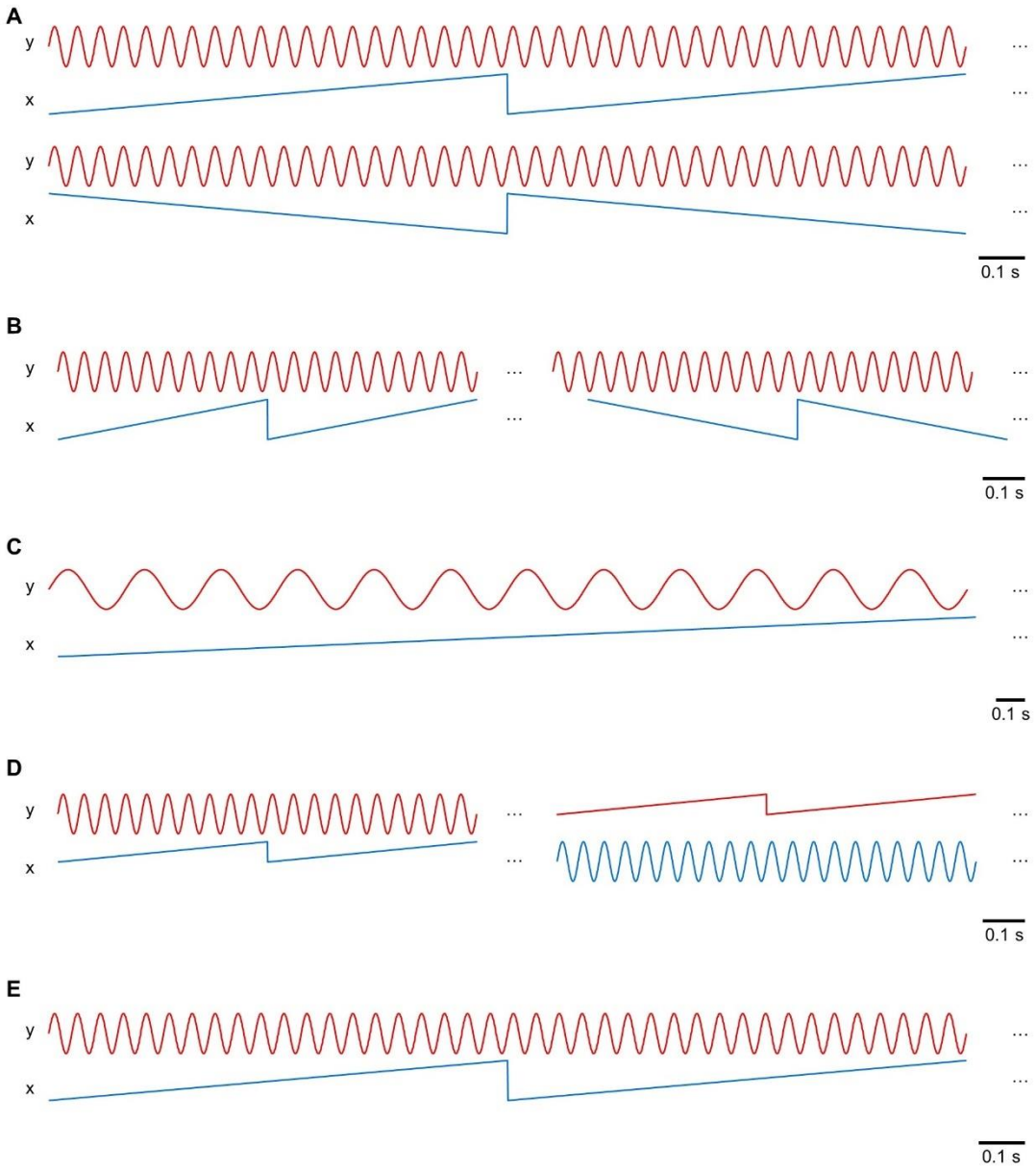

Fig. S25. Electric signals applied to the 2-axis galvo to control the trajectories of the laser. (**A**) Bidirectional linear crawling. (**B**) Bidirectional curvilinear crawling. (**C**) Walking. (**D**) Turning. (**E**) Jumping.

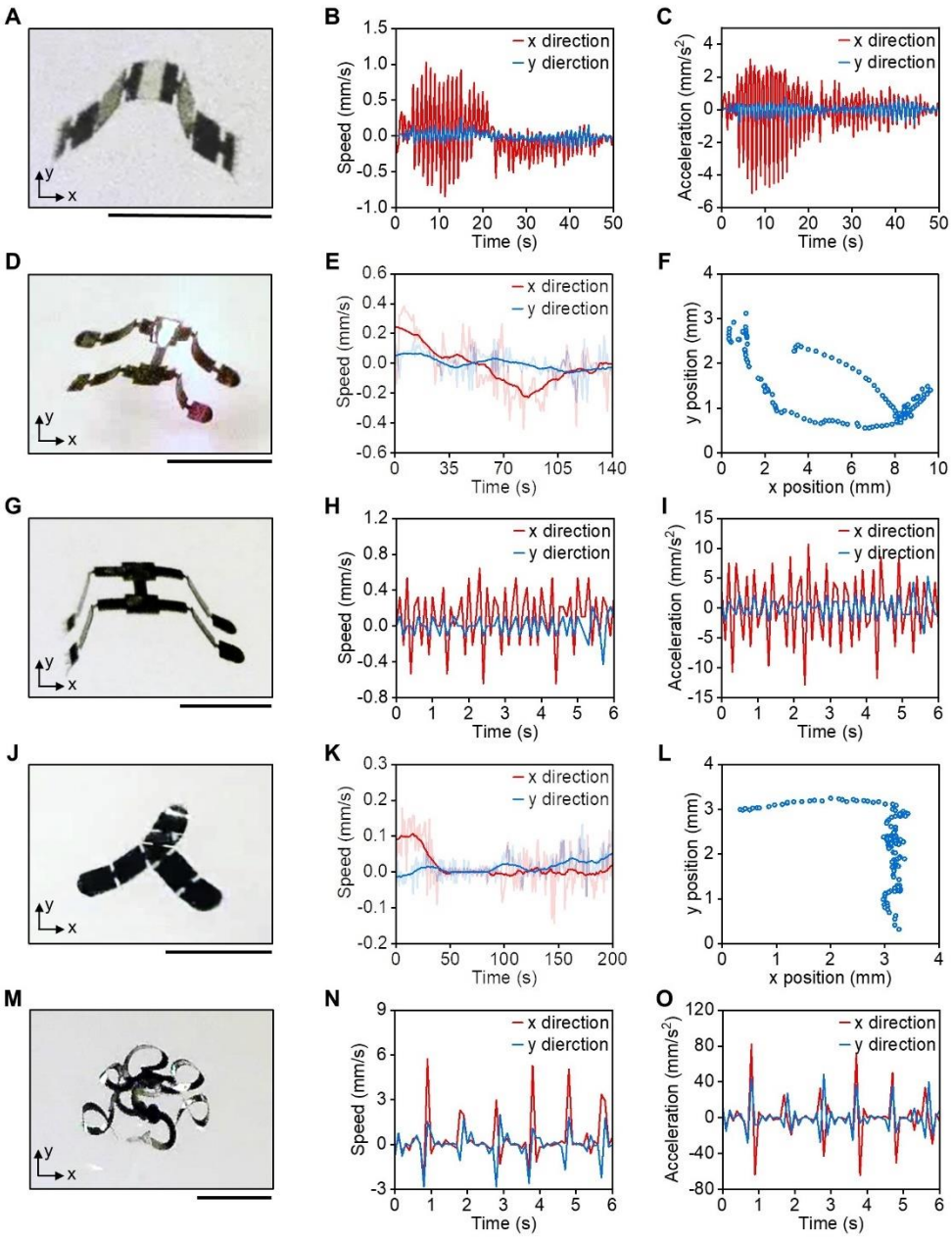

Fig. S26. Additional results of 3D robots with various modes of locomotion. (**A**-**C**)**,** Bidirectional linear crawling: optical image (A), speed (B) and acceleration (C) along x and y directions. (**D**-**F**)**,** Bidirectional curvilinear crawling: optical image (D), speed (E) and trajectory (F) along x and y directions. (**G**-**I**)**,** Walking: optical image (G), speed (H) and acceleration (I) along x and y directions. (**J**-**L**)**,** Turning: optical image (J), speed (K) and trajectory (L) along x and y directions. (**M**-**O**)**,** Jumping: optical image (M), speed (N) and acceleration (O) along x and y directions. Light red and blue curves in (K) and (N) indicate speeds obtained directly from the algorithm. Dark red and blue curves in (E) and (K) indicate speeds after moving average with a window size of 25. Scale bars, 1 mm.

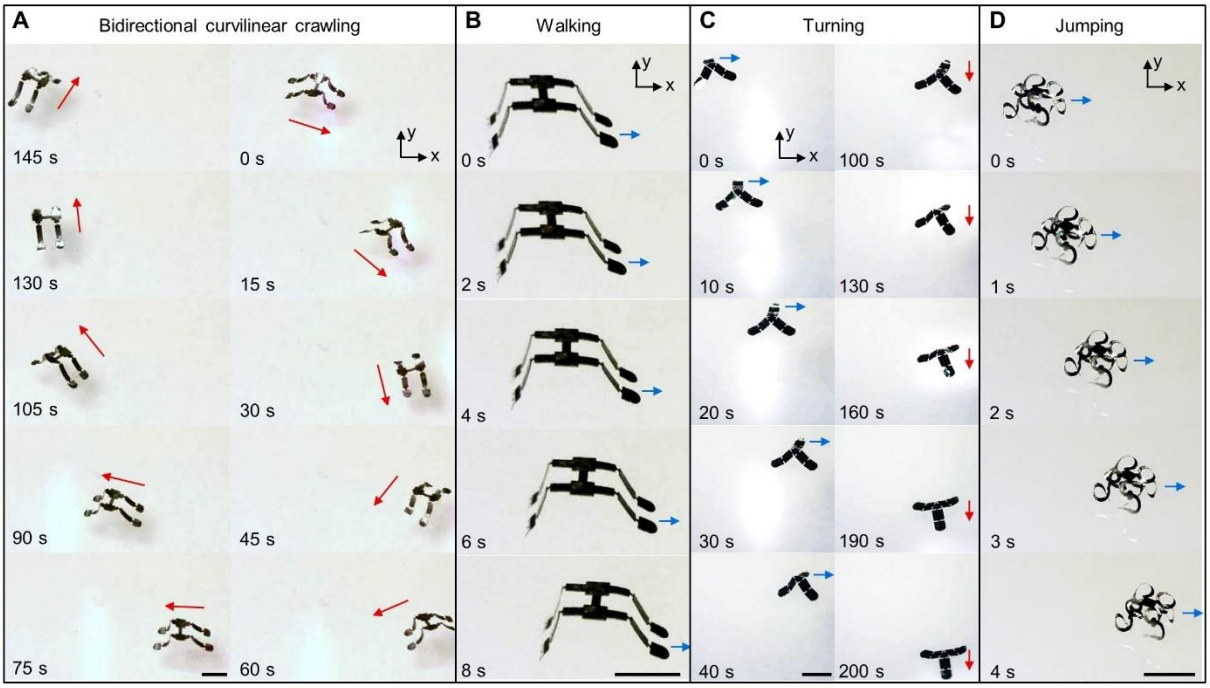

Fig. S27. Positions of robots with various modes of locomotions at different time points. (**A**) Bidirectional curvilinear crawling. (**B**) Walking. (**C**) Turning. (**D**) Jumping. Scale bars, 1 mm.

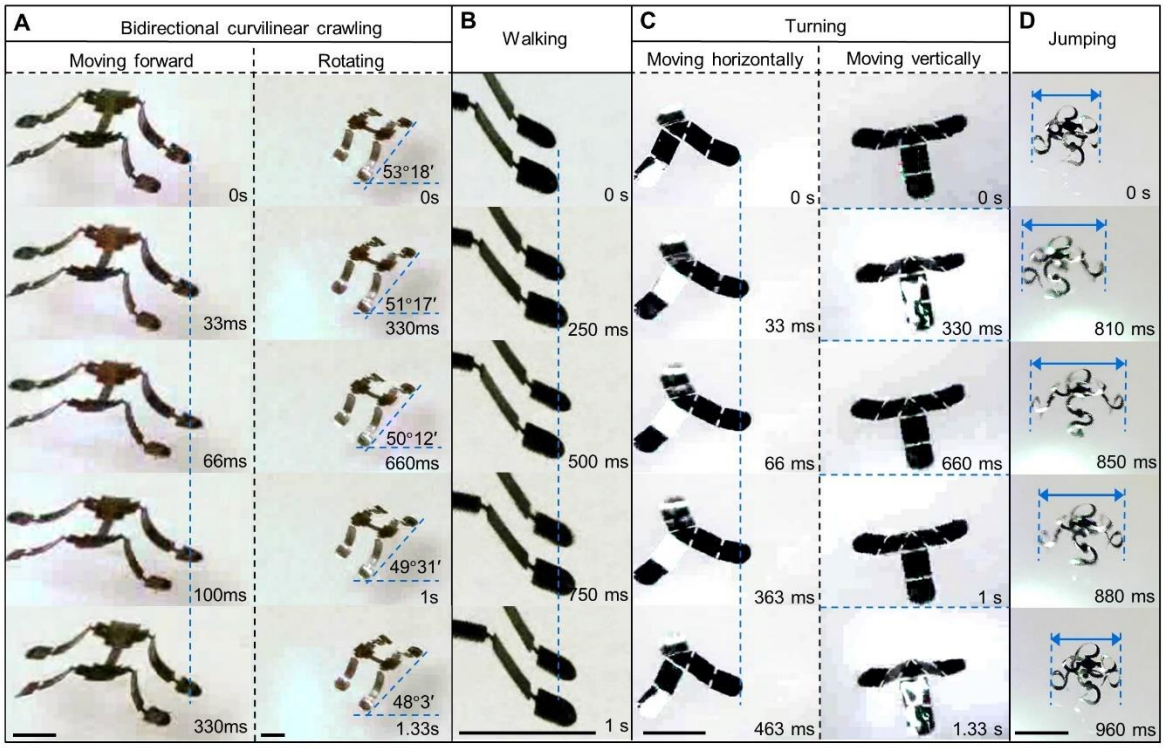

Fig. S28. Optical images robots with various modes of locomotion at different time points. (**A**) Bidirectional curvilinear crawling. (**B**) Walking. (**C**) Turning. (**D**) Jumping. Scale bars, 1 mm.

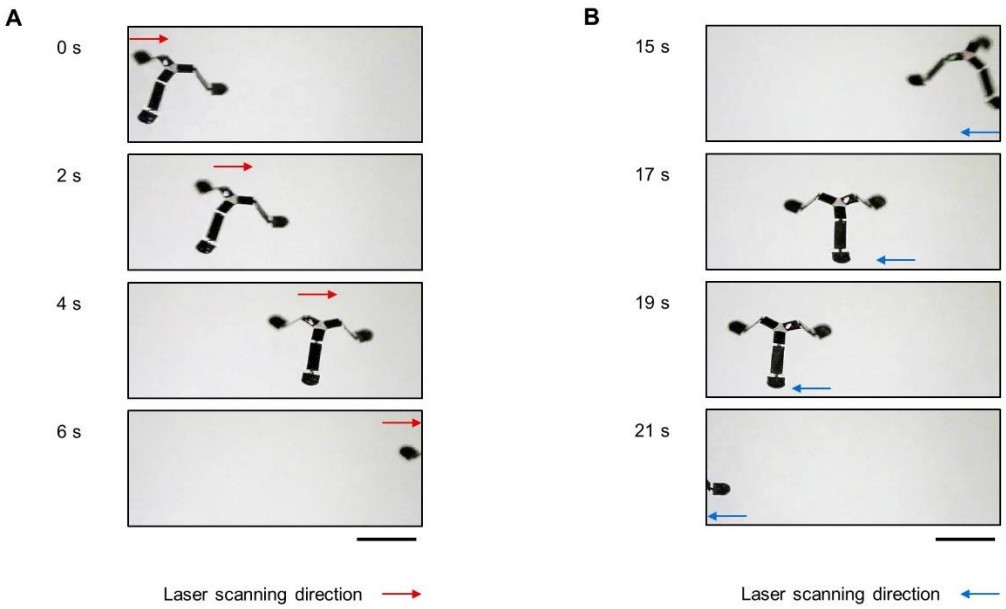

Fig. S29. Optical images of a robot operated on the surface of water under laser scanning. (**A**) From 0 to 6 s, the laser scans from left to right. (**B**) From 15 to 21 s, the laser scans from right to left. Scale bars, 1 mm.

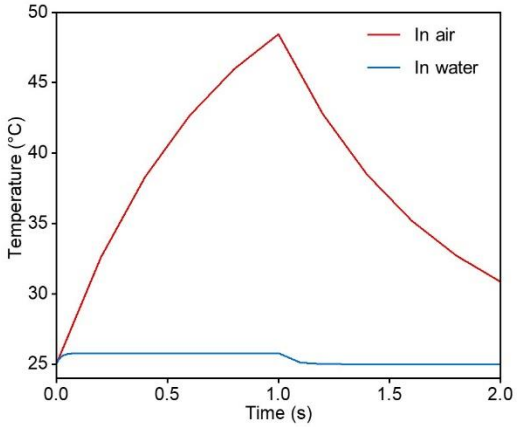

Fig. S30. FEA results of the temperature increase of a robot under laser irradiation. Wavelength: 520 nm, power: 188 mW, spot size: 2.5 mm.

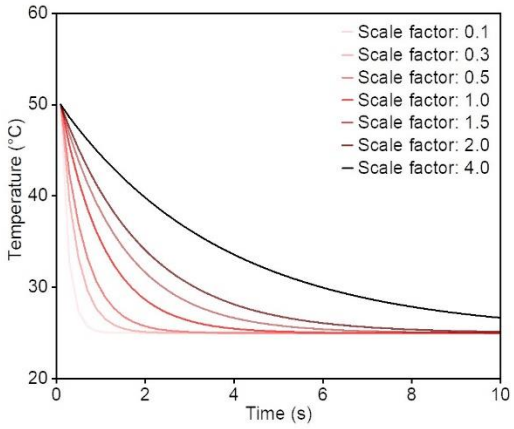

Fig. S31. Dependence of cooling rate on the dimensions of the 3D robot (FEA). Scale factor of 1.0 corresponds to the dimension of the 3D robots in Fig. 2D.

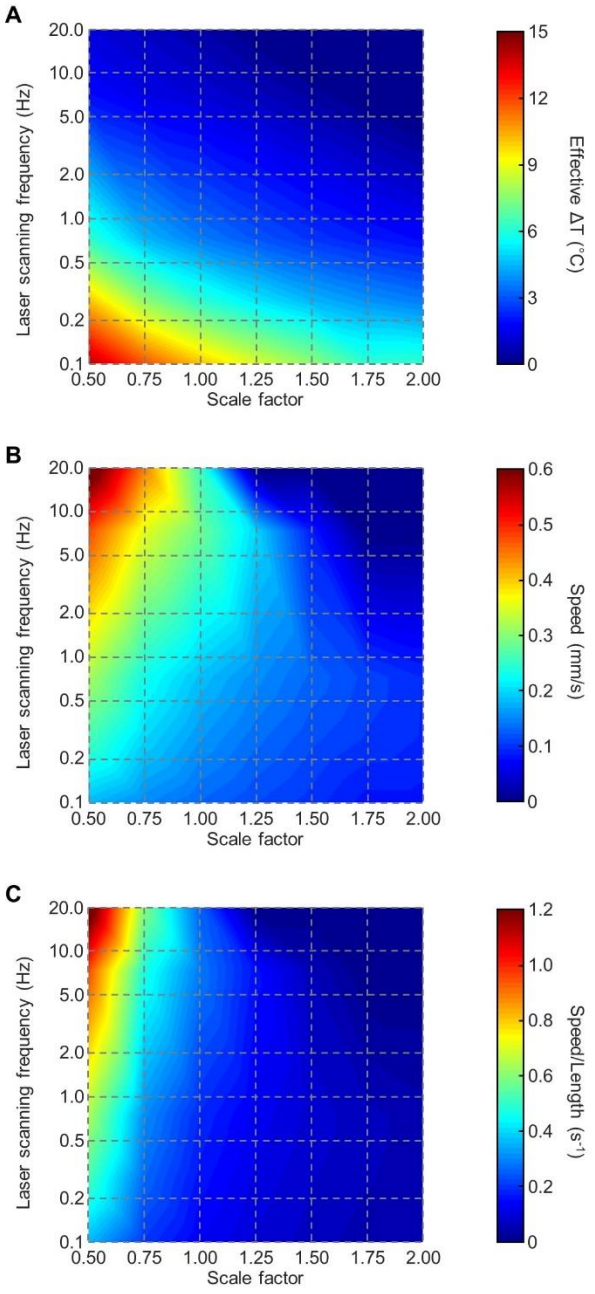

Fig. S32. FEA results of a 3D ribbon at different scales and laser scanning frequencies. (**A**) Effective change in temperature (effective ΔT). (**B**) Speed. (**C**) Speed per body length. Scale factor of 1 corresponds to the 3D ribbon shown in Fig. 2. Data at the intersections of the grey dashed lines are from simulation. Data in other areas are from interpolation.

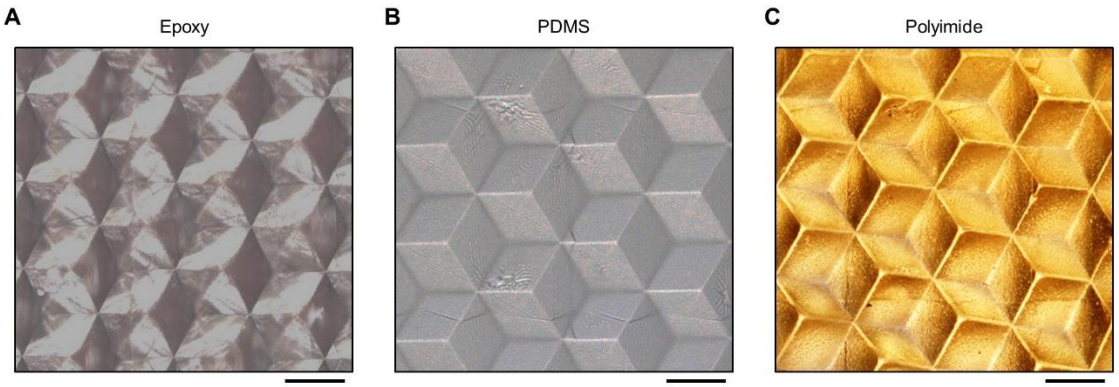

Fig. S33. Optical images of the retroreflector. (**A**) Printed mold in epoxy. (**B**) PDMS structure replicated from the epoxy mold. (**C**) PI structure replicated from the PDMS structure. Scale bars, 100 μm.

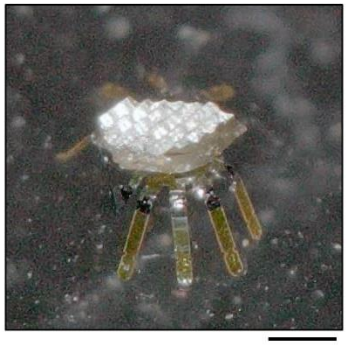

Fig. S34. Optical image of the retroreflector integrated on a robot. Scale bar, 500 μm.

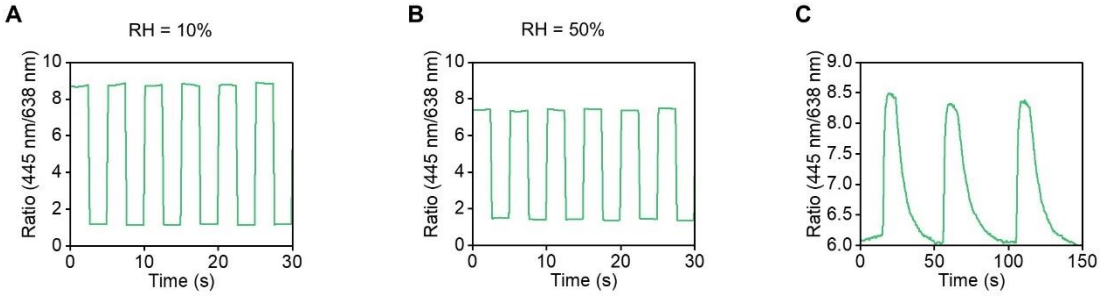

Fig. S35. Additional testing results of the humidity sensor. (**A**-**B**) Ratio between the voltages of the photodetectors for blue and red lasers at RH of 10% (A) and 50% (B). A shutter modulates the laser illumination at a frequency of 0.2 Hz. (**C**) Ratio between the voltages of the photodetectors for blue and red lasers as RH periodically changes between 50% and 10%.

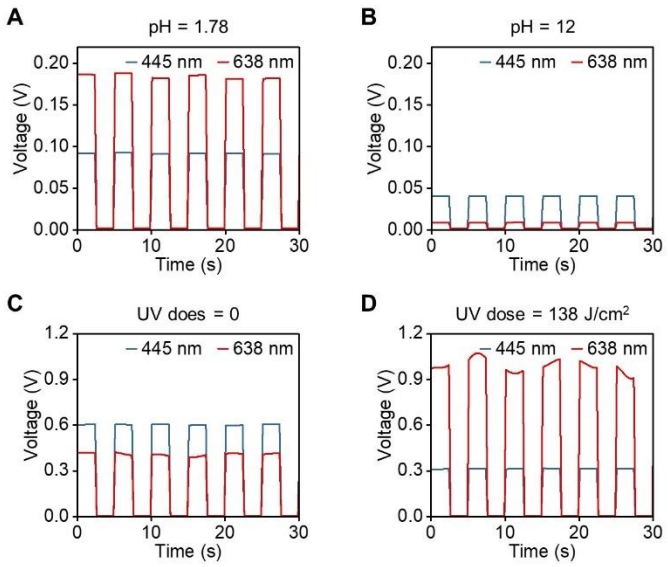

Fig. S36. Additional testing results of the pH and UV sensor. (**A**-**B**) Time-domain output voltages of the photodetectors for blue and red lasers at a pH of 1.78 (A) and 12 (B). (**C**-**D**) Time-domain output voltages of the photodetectors for blue and red lasers at a UV dose of 0 (C) and 138 J/cm^2 (D). A shutter modulates the laser illumination at a frequency of 0.2 Hz.

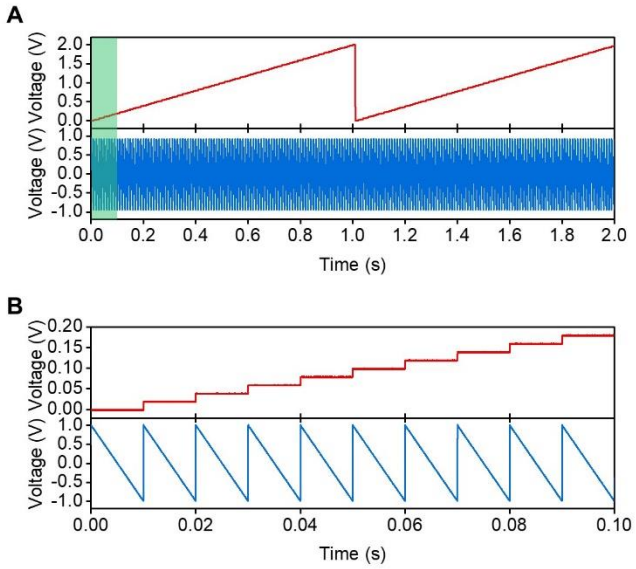

Fig. S37. Input signals to the 2-axis galvo for localizing robots. (**A**) Signal in two cycles. (**B**) Signal in 0.1 s.

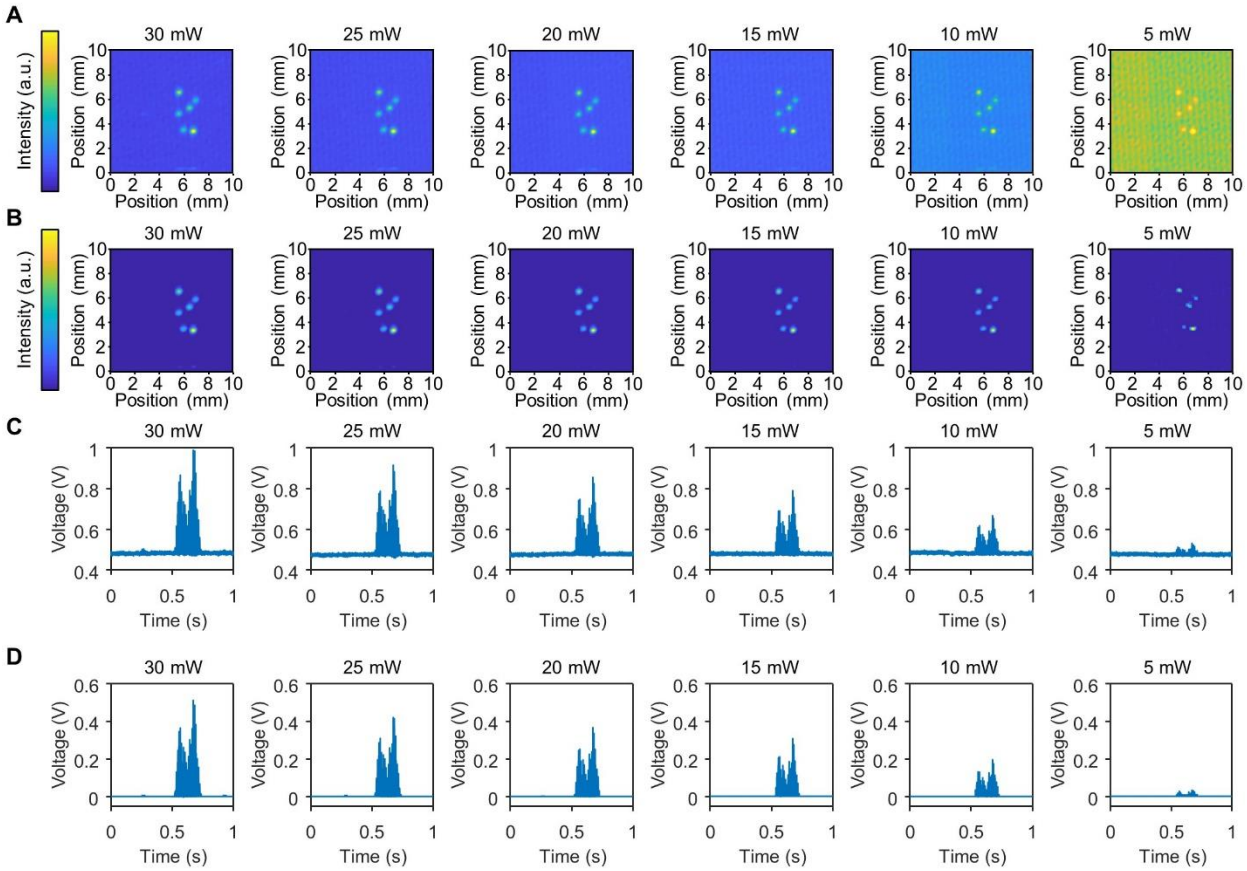

Fig. S38. Localizing six robots through laser-scanning. (**A**-**B**) Intensities of the reflected light at different laser powers in bright (A) and dark (B) environments. (**C**-**D**)**,** Time-domain output voltages from the photodetectors at different laser powers in bright (C) and dark (D) environments.

3. Supplementary Table

Table S1. Key parameters of the robots shown in Fig. 4.

Ref.	Actuation mechanism	Operation environment	Complex 3D & multi-material?	Speed (mm/s)	Length (mm)	Speed/Length (s^{-1})
(37)	Magnetic fields	Terrestrial	Yes	37.3	2.5	14.9
(19)	Magnetic fields	Terrestrial & aquatic	No	65.5	3.7	17.7
(44)	Magnetic fields	Terrestrial	No	250	32	7.76
(45)	Magnetic fields	Terrestrial	Yes	1.67	40	0.04
*(46)**	Magnetic fields	Terrestrial	No	42	0.933	60
*(47)**	Magnetic fields	Aquatic	No	0.18 0.02	0.035 0.0088	5.14 2.27
*(48)**	Magnetic fields	Aquatic	No	12.5	0.3	41.7
(49)	Magnetic fields	Terrestrial	Yes	25.5	5	5.1
*(50)**	Battery power	Aquatic	Yes	64	93	0.69
(51)	Battery power	Terrestrial	Yes	172	45	3.8
(3)	Battery power	Terrestrial	Yes	20	58	0.34
(52)	Battery power	Terrestrial	Yes	4900	104	47
*(53)**	Battery power	Terrestrial	Yes	12	40	0.3
(54)	Chemical reactions	Aquatic	No	0.12	0.02	6
*(26)**	Chemical reactions	Aquatic	Yes	1.6	1	1.6
(21)	Chemical reactions	Aquatic	No	0.005	0.025	0.2
(55)	Chemical reactions	Aquatic	Yes	2.34	3	0.78
(30)	Light exposure 532 nm, 10^8 mW/cm^2	Terrestrial	No	0.38	0.06	6.3
(29)	Light exposure 660 nm, 2.2×10^8 mW/cm^2	Terrestrial	No	0.02	0.03	0.67
(56)	Light exposure ultra-violet and white light ~1000 mW/cm^2	Aquatic	No	0.142	26.3	0.0054
(57)	Light exposure 385 nm, 150 mW/cm^2	Terrestrial	No	0.25	8	0.031
(58)	Light exposure 532 nm, ~70000 mW/cm^2	Terrestrial	No	0.5	14.5	0.034
(59)	Light exposure 808 nm, 280 mW/cm^2	Terrestrial	No	16	34	0.47
(60)	Light exposure 532 nm Up to ~4700 mW/cm^2	Aquatic	No	0.3	14	0.02
(20)	Light exposure NIR light, 250 mW/cm^2	Terrestrial	No	1.75	14.5	0.12
(61)	Light exposure 447 nm, 8.9 mW/cm^2	Terrestrial	No	1.1×10^{-4}	16.5	6.7×10^{-6}
(22)	Light exposure 785 nm, 10000 mW/cm^2	Aquatic	No	0.001	0.07	0.014
(62)	Light exposure 520 nm up to 4500 mW/cm^2	Terrestrial	No	0.37	15	0.025

References marked with '*' correspond to robots that can change directionality during movement in a controllable way.

4. Supplementary Movies

Movie S1. Stability of the robots.

Movie S2. Various motion modalities of the robots.

Movie S3. Selective activation of one crab structure.

Movie S4. Directional locomotion of the crab structure.

Movie S5. Edges and nodes of the ribbon structure detected by the customized algorithm.

Movie S6. Directional locomotion of the ribbon structure at different laser-scanning frequencies.

Movie S7. Robot with bidirectional linear crawling locomotion.

Movie S8. Robot with bidirectional curvilinear crawling locomotion.

Movie S9. Robot with walking locomotion.

Movie S10. Robot with turning locomotion.

Movie S11. Robot with jumping locomotion.

Movie S12. Robot operated on the surface of water.